Electron-electron correlations in fullerene C_{60} probed by incoherent scattering of x rays

C. Petrillo,[1] F. Sacchetti,[1] A. Orecchini,[1] R. De Renzi,[2] and M. Riccó[2]
[1]*Dipartimento di Fisica, Universitá di Perugia, I-06123 Perugia, Italy and CNR-INFM CRS-Soft, Roma, Italy*
[2]*Dipartimento di Fisica, Universitá di Parma and CNISM, I-43100 Parma, Italy*
(Received 9 March 2006; revised manuscript received 3 July 2006; published 10 August 2006)

The static structure factor of electrons in fullerene has been obtained by a properly designed x-ray diffraction experiment. Due to the intense diffuse scattering caused by the orientational disorder of the C_{60} molecules in fullerene, the experiment presented several difficulties. Nonetheless, the data were accurate enough to provide an estimate of the exchange-correlation energy and to make a valuable comparison of the static structure factors of fullerene and diamond. The observed value of the exchange-correlation energy, which is larger in fullerene than in diamond, suggests a clear link between carbon polymorphism and dynamic electron correlations. The experimental data of static structure factor of fullerene, together with the derived exchange-correlation contribution to the cohesion and the pair-correlation function, offer an interesting test on the validity of the local-density treatment of the electron correlations in solids.

DOI: 10.1103/PhysRevB.74.085404 PACS number(s): 61.10.−i, 71.45.Gm

I. INTRODUCTION

Experimental data on the ground-state energy of an elemental crystal can be obtained from a complete x-ray scattering study of the system, namely, a Bragg diffraction experiment (coherent contribution) coupled to the measurement of the energy-integrated incoherent (Compton) cross section. The relationship between the ground-state energy and the cross section of the scattering process in a crystal was discussed in Ref. 1 under a nonrelativistic treatment of the coupled electron-photon system, and for photon energies restricted to the x-ray range. Specifically, x-ray scattering measurements enable us to distinguish between static and dynamic contributions to the total energy of the crystal ground state.[1,2] Static contributions, that is, the electron-electron Hartree energy and the electron-nucleus interaction energy, depend on the charge density and can be obtained by accurate Bragg diffraction experiments[2] where the structure factors of the crystal, that is, the series coefficients of the electron-density expansion in the Fourier lattice series, are measured. On the contrary, the dynamic contribution to the electron-electron interaction energy, that is, the exchange-correlation energy, is provided by the measurement of the incoherent or non-Bragg signal.[1,2]

The incoherent cross section is proportional to the electronic static-structure factor $S(\boldsymbol{Q})$, which, in turn, is related to the exchange-correlation energy per atom through

$$E_{xc} = \frac{e^2}{8\pi^2} \int d\boldsymbol{Q} \frac{S(\boldsymbol{Q}) - Z}{Q^2},$$

$\boldsymbol{Q}$ being the exchanged wave vector and Z the atomic number of the system. The function $S(\boldsymbol{Q})$ is also usefully written as the Fourier transform of the density-weighted two-body correlation function $g(\boldsymbol{r},\boldsymbol{r}')$ which describes, in real space, the dynamic correlations between pairs of interacting electrons and, given the purely two-body nature of the Coulomb interaction, it fully accounts for the collective behavior of the many-electron system. The fundamental role of the pair-correlation function has been enlightened by the density-functional theory[3] (DFT) where the exchange-correlation energy is conveniently viewed as the interaction between an electron and the charge of its Fermi-Coulomb hole.

Considering that the quantitative account of the electron correlations in many-electron systems still represents a challenge, and that the most striking properties of real solids are poorly or not at all accounted for by single-particle schemes, access to experimental data on fundamental ground state observables, like total energy and pair-correlation function, should be taken as highly valuable. Moreover, x-ray scattering experiments enable us to distinguish the solid-state dependences of conduction-electron density and pair-correlation function, against the continuous and isotropic scheme of the homogeneous interacting electron gas model.[3] This feature is of special relevance when assessing the validity of the local density approximation (LDA) to the DFT. Indeed, the LDA exploits the homogeneous interacting electron gas as a reference system for local modeling of the density-dependent energy E_{xc} in the solid.

The suitability of incoherent scattering of x rays as a sensitive tool of the electron-electron correlations has been demonstrated by experiments in light elemental crystals, namely, Be,[4] Al,[5] Si,[6] C in the diamond phase,[7] and more recently, LiF.[8] Extended sets of pair-correlation-function data were obtained for the three prototypical systems, namely, metallic Be,[4] the covalent-bond insulator C (diamond),[7] and the ionic-bond insulator LiF.[8] The experimental results clarified the role of the electron-density distribution either in determining the size of the Fermi-Coulomb hole surrounding each electron or in bringing about the binding in the solid. Measured widths of the Fermi-Coulomb hole turned out to be ~0.6 Å in diamond and LiF, whereas a value of ~0.9 Å was observed in Be. Moreover, it was found that the cohesive energy is dominated by the exchange-correlation contribution in Be and diamond, whereas only a 50% contribution resulted in LiF, the remaining 50% of the cohesive energy being due to the one-electron-density deformation. Quite surprisingly, and contrary to the simple expectation about a jellium model working properly in simple metals only, the pair-correlation functions, and hence the dynamic correlations

among valence electrons, were found to be rather well described by the jellium model not only in Be but also in insulating diamond. The effects of the one-electron density inhomogeneity, negligible in Be and diamond, were remarkable in LiF where the experimental static structure factor of the valence electrons showed clear differences from the homogeneous interacting electron gas at the corresponding density. The experimental data in LiF were, however, well reproduced by an electron-density-weighted average of the pair-correlation functions of the homogeneous electron gas. This result could be possibly taken as experimental evidence of the capability of LDA-based prescriptions to describe the electron correlations in an ionic system, highly nonhomogeneous, like LiF.

The circumstance that only a limited number of crystalline systems was investigated can be partly explained by the technical requirements which accompany this difficult kind of x-ray experiment. First of all, a good-quality single-crystal sample is necessary for an accurate definition of the path in the reciprocal lattice. Indeed, the path should avoid as many Bragg points as possible and should be traced starting from any high-symmetry direction. Since crossing a Bragg point would obscure completely the sought-for incoherent signal, a relatively simple crystallographic structure of the sample is welcome. The availability of a good-quality single crystal can be additionally exploited for the ordinary Bragg-diffraction study, leading to the knowledge of the charge density and hence of the Hartree contribution to the total energy. A further constraint, which prevents the study of heavy elements, is represented by the considerable increase of the photoabsorption cross section with an increase of the atomic number. However, confining the experiments to light elements, which have a relatively small fraction of core electrons, enables us to more easily obtain the valence-electron contribution to the pair-correlation function. An additional limitation to these experiments comes from the thermal-nuclear motion whose unavoidable contribution to the scattering has to be subtracted. Therefore, experiments are better carried out in systems characterized by a high Debye temperature. A good example is diamond, whose high Debye temperature made the corrections for thermal diffuse scattering (TDS) fairly small.

Diamond also has a special meaning as one of the ordered allotropes of carbon, besides graphite and the archetypical fullerene C_{60}. The variety of coordination that carbon can sustain, namely, the diamondlike sp^3, the graphitelike sp^2, and even sp, makes it a system with unique characteristics. The investigation of the carbon allotropes, in particular carbon fullerenes as well as carbon nanotubes, is a research topic receiving considerable attention both at a fundamental physics level[9] and for potential applications as nanoscale devices and biosensors.[10] Carbon fullerenes, other than being characterized by an extremely high symmetry, exhibit a huge variety of physical properties ranging from superconductivity to ferromagnetism. Taking advantage of the already available data on diamond, we believe that the x-ray incoherent scattering investigation of the carbon allotropes, graphite and fullerene C_{60}, would emphasize the role of the dynamic-electron correlations on the stability of the ground state for the different sp^3 and sp^2 hybridization states and, correspondingly, crystal structures. In insulating diamond, the crystal stability is largely ensured by the exchange-correlation contribution to the cohesive energy, which amounts to $\sim 4.4 \pm 0.2$ eV/atom[7] against the electrostatic Hartree contribution[2] equal to 1.6 ± 0.2 eV/atom. The investigation of graphite and fullerene, aimed at identifying possible changes of $S(\boldsymbol{Q})$, and hence of E_{xc} and $g(\boldsymbol{r},\boldsymbol{r}')$, with respect to diamond, would help in clarifying the role of the exchange-correlation energy on the carbon polymorphism.

With the exception of diamond, all the carbon allotropes are far from being optimal samples for the proposed x-ray investigation. The preferred candidate was fullerene C_{60} for which good-quality crystals can be grown. However, remarkable experimental difficulties were expected also with this sample because of the intrinsic molecular orientational disorder of the C_{60} units, which causes an intense diffuse-scattering contribution, potentially exceeding the diffuse-scattering term due to $S(\boldsymbol{Q})$ itself. Because of the orientational disorder, the incoherent x-ray scattering experiment was at the limit of the technical performances and the demand for accuracy was extremely high. Considerable help came from the existing data on diffuse scattering from disorder and TDS in fullerene, which were collected in neutron diffraction experiments.[11–13] The neutron measurements, which probe the nuclear correlations only, allowed the evaluation of the orientational disorder and TDS contributions to the electronic diffuse scattering, thus providing a proper correction of the experimental x-ray data for these effects. The incoherent x-ray-scattering experiment was confined to the study of the room temperature disordered phase of fullerene, where the effects of the orientational disorder were smoothed by the thermal motion. Indeed, the partially ordered structure appearing at a temperature below 260 K would have made the study of the diffuse scattering even more difficult.

II. EXPERIMENT AND DATA ANALYSIS

The incoherent and energy-integrated x-ray-scattering experiment in a crystalline sample provides a measurement of the differential cross section per atom

$$\frac{d\sigma}{d\Omega} = \frac{1+\varepsilon\cos^2(2\vartheta)}{2}\left[r_0^2\left(\frac{k}{k_0}\right)^2 S(\boldsymbol{Q}) + \left(\frac{d\sigma}{d\Omega}\right)_{TDS} + \left(\frac{d\sigma}{d\Omega}\right)_{dis} + \left(\frac{d\sigma}{d\Omega}\right)_{Bragg}\right], \quad (1)$$

where r_0 is the classical electron radius, ε is a polarization factor, which is equal to 1 for the present experimental configuration, k_0 and k are the wave vectors of the incoming and outgoing photon, and 2ϑ is the scattering angle. The validity of Eq. (1) was thoroughly discussed in Refs. 1 and 2. Here we are reminded that it is based on the assumption that an efficient integration over all the inelastic scattering events, with the energy of the diffused photon comprised within a small range around $\hbar ck$, is performed. Also, it holds for photon energies largely in excess of any absorption edge of the sample. The experimental cross section is proportional to the electronic static-structure factor $S(\boldsymbol{Q})$, although it contains the *unwanted* contributions from TDS and residual Bragg

scattering, plus a diffuse-scattering term which originates from disorder. Indeed, any defect present in a crystal gives rise to a diffuse-scattering contribution, which, generally, is negligible in high-quality monoatomic single crystals. In a molecular crystal, additional diffuse scattering is brought about by the random orientation of the molecular units, and this is what occurs in fullerene, where the C_{60} molecules are randomly oriented.[11–13] Because of the transition to a partially ordered structure, which takes place at $T \sim 260$ K in C_{60}, we preferred to carry out the x-ray measurements at room temperature. Indeed, even though the TDS is larger at room temperature, the lattice has a higher symmetry and, consequently, the number of Bragg peaks is reduced, which is a clear advantage for the measurements. The Bragg contribution must be avoided also at the level of tails, because of its intensity that is exceedingly larger than all other terms, and because of its unknown shape, which prevents a proper subtraction from the data.

The room-temperature experiment was carried out on a C_{60} single crystal with a size about $1 \times 1.5 \times 0.8$ mm. C_{60} single crystals were grown using an open-vapor transport technique. High-purity C_{60} powder (99.9% from MER Corporation, Tucson, Arizona) was doubly vacuum sublimed and subsequently introduced in a multizone horizontal tube furnace whose temperature profile can be accurately prearranged (exposure to air of C_{60} was avoided during all these operations). High-purity dry He was flowed through the furnace while its temperature was slowly raised to approach the C_{60} sublimation temperature ($\sim$843 K) and the temperature profile was set as described in Ref. 14. After 3–5 days, C_{60} single crystals of millimeter size could be collected at the growth zone of the furnace. The quality of the sample selected for the present experiment was checked by x-ray Bragg diffraction and specific rocking curves and coupled (ω-2ϑ) scans were measured. The crystal was found to be of good quality, with $\sim$0.2° mosaic spread. As an example, the rocking curve of the (222) reflection and the (ω-2ϑ) scan along the [110] direction are shown in Fig. 1. The incoherent scattering data were collected using a sealed-tube diffractometer, properly adapted to measure diffuse scattering. A normal-focus Ag anode was mounted for the experiment. The energy of the Ag $K\alpha$ radiation (22.10 keV) is, indeed, higher than the K edges of carbon and high enough to minimize the absorption through the sample. Downstream the x-ray beam, a (002) pyrolitic graphite flat monochromator with 0.5° mosaic spread was employed to reduce the Bremsstrahlung and the $K\beta$ contamination of the incoming beam. The incoming beam was vertically collimated by means of a tungsten Soller slit with 3° divergence, while the horizontal angular divergence was defined by a 0.5 mm slit inserted before the monochromator and at 100 mm from the anode. The beam size at the sample position was 1×10 mm, with 0.6° horizontal angular divergence. A standard NaI:Tl scintillator detector coupled to a photomultiplier was used for photon collection. The energy resolution of the detector was $\sim$5 keV with the energy bandwidth set from 10 to 30 keV. With the chosen setting, a good rejection of the half-wavelength contamination from the photon source, which was operated at 50 kV for the best efficiency, was achieved. To reduce the background due to air scattering, the sample

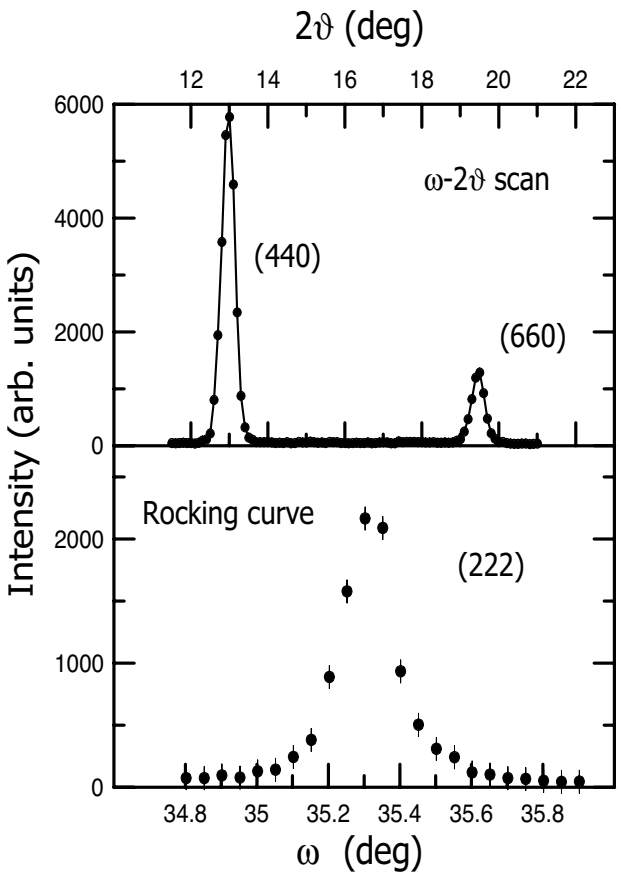

FIG. 1. Rocking curve of the (222) reflection of C_{60} (lower panel): the raw intensity data are shown versus the rocking angle ω. Coupled (ω-2ϑ) scan along the [110] direction of the C_{60} crystal (upper panel): the raw intensity data are plotted vs the scattering angle 2ϑ.

was mounted inside a cylindrical vacuum chamber (110 mm diameter) equipped with a round beryllium window, thin enough (250 μm) for the incident and scattered x-ray beams to go through without suffering appreciable attenuation. A Soller collimator, 100 mm long with Mo blades, 1 mm apart, and a full aperture 12×12 mm^2, was inserted between the vacuum chamber and the photon detector.

The shape of the crystal was not regular enough to enable reliable corrections for scattering-volume effects, as required for a proper treatment of data collected along scans involving an ω rotation at the sample. Therefore, the sample was maintained in a fixed configuration, that is, only 2ϑ scans in the reciprocal lattice, which correspond to constant sample volume during the scan, were possible. Each scan was executed by missetting the crystal off a known orientation and rotating the detector arm around the fixed sample. The data were collected along three different 2ϑ scans starting from different orientations of the sample, that is, from three nonequivalent crystallographic planes. For each direction, the sample was carefully oriented to minimize the distance between the path line and the reciprocal lattice points. As an example, the path in the reciprocal lattice described by one of the scans is shown in Fig. 2 as an inset for the $(1\bar{1}0)$ reciprocal lattice section. As is apparent from the figure, most of the Bragg

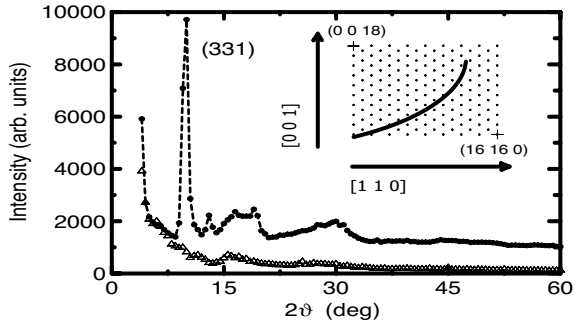

FIG. 2. Raw-intensity data measured along the reciprocal lattice line (shown in the inset) vs scattering angle 2ϑ in C_{60} (dots). The attenuation-corrected background to be subtracted from the intensity data is also shown (empty triangles). The dashed line is a guide to the eye. Inset: $(1\bar{1}0)$ reciprocal lattice section of C_{60} showing the path line followed by one of the 2ϑ scans.

peaks were not intercepted by the prepared path line. Similar scans were carried out for the other two sample orientations, namely, the crystal was rotated by 45° and 90° around the [100] axis. Each 2ϑ scan covered the angular range from 4° to 60° with a 0.5° angular step, and was repeated four times to ensure at least 2% statistical accuracy on the weakest intensity points. The background was measured removing the sample and performing the same 2ϑ scans as with the sample. Additional background measurements were carried out by substituting the sample with absorbing lead.

To obtain the electron static-structure factor $S(\boldsymbol{Q})$, the measured intensity data were first corrected for background by following the standard procedure applied to experiments of the same kind.[7,8] As an example, in Fig. 2 the raw intensity scattered from the sample and collected along the same scan as shown in the inset, is compared with the attenuation-corrected background intensity.

Multiple scattering processes taking place inside the sample also affect the measured intensity and must be subtracted. However, this contribution, which is well represented by a very smooth and almost Q-independent function, was negligibly low for the present C_{60} sample. The contamination of the intensity due to possible tails of Bragg peaks intercepting the path in the reciprocal lattice was carefully checked for each of the scans and accordingly subtracted from the data. The critical point of the data analysis was, however, the subtraction of the TDS and the diffuse contribution due to the molecular disorder. The background-free intensity was therefore corrected for the angle-dependent sample attenuation and put on absolute scale by internal normalization to the high-Q limit of the cross section, as given by

$$\lim_{Q\to\infty}\frac{d\sigma}{d\Omega}=r_0^2\frac{1+\varepsilon\cos^2(2\vartheta)}{2}\left[\left(\frac{k}{k_0}\right)^2 S_{at}(\boldsymbol{Q})+\frac{f^2(Q)}{b^2}\left(\frac{d\sigma}{d\Omega}\right)_{neu}\right]. \tag{2}$$

In Eq. (2) the static-structure factor of the solid was replaced by that of the free atom $S_{at}(\boldsymbol{Q})$, which is a meaningful approximation in the high-Q limit, whereas the diffuse scattering contributions due to the unknown TDS and molecular-disorder terms were accounted for by the neutron cross section as measured in Ref. 13, properly scaled for the squared ratio of the atomic-scattering factor $f(Q)$ to the neutron-scattering length b. We remark that, since the neutron-diffraction data of Ref. 13 were collected on a powdered sample of fullerene, the approximation for the thermal and molecular-disorder diffuse contributions, as contained in Eq. (2), amounts to substituting possible direction-dependences of the cross section by their spherical average. In the high-Q limit and for the normalization purposes of Eq. (2), use of the spherical average was considered quite a satisfactory approximation. The free-atom static-structure factor $S_{at}(\boldsymbol{Q})$ and the atomic-scattering factor $f(Q)$ were obtained from the configuration interaction calculations of Ref. 15, which represent the best estimates presently available in literature. The experimental data collected along the three different directions in the reciprocal lattice were separately normalized and then averaged with respect to the different symmetry directions with weights given by the multiplicity. This provides a sort of spherically averaged differential cross section, from which the spherical average of the static-structure factor, namely, $S(Q)$, could be obtained by direct subtraction of the Q-dependent spherical average of the diffuse terms as provided by the neutron-diffraction experiment.[13] The cross section obtained by direct subtraction was, however, affected by a notable residual oscillation superimposed to the expected trend. This was a clear indication that the unwanted diffuse term, although approximated at best by the neutron data at every exchanged wave vector and not only in the high-Q limit, was not efficiently subtracted with the applied procedure. To overcome the problem of the residual oscillations and to extract a clean $S(Q)$ from the measured data, we observed that the cross section is the sum of positive-defined terms. In particular, the diffuse term $\left[\left(\frac{d\sigma}{d\Omega}\right)_{TDS}+\left(\frac{d\sigma}{d\Omega}\right)_{dis}\right]\sim r_0^2\frac{f^2(Q)}{b^2}\left(\frac{d\sigma}{d\Omega}\right)_{neu}$ is positive defined, which implies that it does not oscillate around the zero level and that any residual oscillation would lie wholly above the expected curve of the $S(Q)$ contribution. Based on these observations, the electronic contribution was derived from the data as the set of the experimental points lying at the bottom of the intensity oscillations. This procedure offered a rationale for the selection of acceptable data and provided a new set, which was rather depleted of data over the range $Q\leq 5$ Å^{-1}, where the residual oscillations were larger. The resulting spherical average of the electronic structure factor of C_{60} is plotted in Fig. 3, which compares the experimental data with the companion results in diamond and the carbon atom. A fit to the experimental data of $S(Q)$ in C_{60} was carried out by using the Gaussian-based representation

$$S^{fit}(Q)=Z-\sum_{i=1}^{4}a_i\exp[-b_iQ^2], \tag{3}$$

where a_i and b_i are free parameters of the fit with the constraint $\Sigma_{i=1}^4 a_i=Z$. The curve resulting from the best fit of the data is also shown in Fig. 3 as a continuous line.

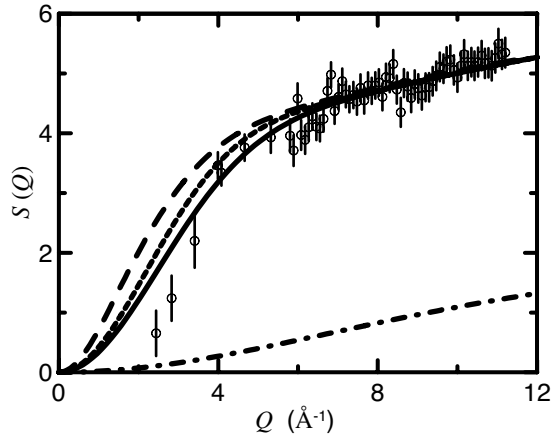

FIG. 3. Electronic static-structure factor $S(Q)$ vs exchanged wave vector Q in C_{60} and diamond. Circles: spherical average of the C_{60} experimental data (see text). Full line: best fit curve to the C_{60} experimental data, according to Eq. (3). Dot-dashed line: calculated core-electron contribution in C_{60}. Short-dashed line: spherical average of the diamond experimental data (Ref. 7). Dashed line: calculated free-carbon atom (Ref. 15).

An internal check of the reliability of the whole procedure consisted in using the fitted function $S^{fit}(Q)$ to derive, in turn, the effective total-diffuse contribution by direct subtraction from the measured cross section Eq. (1). The diffuse term $S^{dis}(Q)$ resulting from this procedure is plotted in Fig. 4 in comparison with the data measured in the neutron-diffraction experiment.[13] The overall agreement between the present *indirect* estimate of the diffuse term and the experimental neutron data is appreciable especially over the region of higher-Q values, that is, where the cross section is less sensitive to the details of the actual orientational disorder and the averaging procedure. This result was taken as a satisfactory check of the reliability and consistency of the present data-correction procedure.

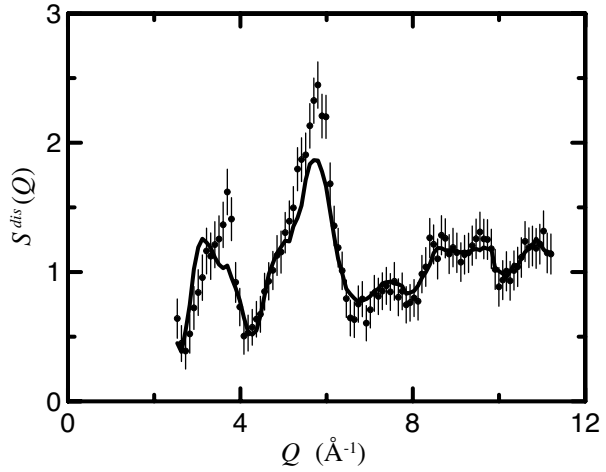

FIG. 4. Static-structure factor $S^{dis}(Q)$ arising from the diffuse scattering associated to TDS and molecular orientational disorder in C_{60}. Continuous line: data measured in the neutron-diffraction experiment of Ref. 13. Dots: data derived from the present x-ray experiment as an internal consistency check of the data-analysis procedure (see text).

III. DISCUSSION

The static-structure factor of the valence electrons $S_{val}(Q)$ was obtained by subtracting from $S(Q)$ the core contribution calculated according to Ref. 16 and shown in Fig. 3. As already suggested by Fig. 3, $S_{val}(Q)$ was found to be slightly lower in fullerene than in diamond over the low-Q region. Consequently, the contribution to the cohesive energy arising from the exchange-correlation effects was expected to be higher in fullerene than in diamond. The experimental evaluation of this energy contribution is possible only through a measurement of $S(Q)$ and exploiting the relationship

$$E_{coh}^{xc} = \frac{e^2}{2\pi} \int [S_{at}(Q) - S(Q)] dQ. \tag{4}$$

Since $S_{at}(Q)$ is generally greater than $S(Q)$, the exchange and correlation contribution to the cohesive energy is positive and sizable. The contribution of the core electrons to E_{coh}^{xc} is negligible, therefore all the effects come from the valence-electron static-structure factor, although a decomposition into core and valence contributions is not formally exact. Because of the limited quality of the present data, mostly due to the unknown diffuse disorder terms, we did not try to derive E_{coh}^{xc} directly from the experimental data, which do not span the explored Q range in a continuous way, but we made use of the fitted functions $S^{fit}(Q)$. The use of fitted curves to carry out integrals like in Eq. (4) makes the calculation more straightforward and provides rather accurate results. This point was specifically checked applying Eq. (3) to fit the *virtually exact* atomic static-structure factor given in Ref. 15. An exchange-correlation energy per atom equal -5.63 ± 0.02 Ry/atom resulted from the integration of the fitted curve, which was, within the errors due to the fit, in perfect agreement with the value obtained by direct integration of the data of Ref. 15. We also note that possible errors due to a nonaccurate fitting of the static-structure factors do not significantly affect the value of E_{coh}^{xc}, which results from the difference between the solid and atom energies, that is, two quantities separately affected by the same error.

Making use of the curve $S^{fit}(Q)$ fitted to the C_{60} data, an exchange-correlation energy equal to -6.27 ± 0.10 Ry/atom was obtained with a corresponding contribution to the cohesive energy equal to $+0.64 \pm 0.10$ Ry/atom (8.7 eV/atom). The latter data must be compared directly with the corresponding value in diamond, which was found to be +0.32 Ry/atom (4.35 eV/atom). As already suggested by the shape of $S(Q)$, the exchange-correlation energy contribution in fullerene is appreciably larger than in diamond. Unfortunately no accurate measurement of the scattering factor $f(Q)$ in fullerene is available, which prevents the evaluation of the Hartree contribution to the cohesive energy. Moreover, no experimental estimate of the cohesive energy of fullerene seems to be available. Despite the limited experimental data on the ground-state energy of fullerene, the difference between E_{coh}^{xc} in fullerene and diamond appears to be meaningful and it can be relevant in defining the relative stability of the two systems.

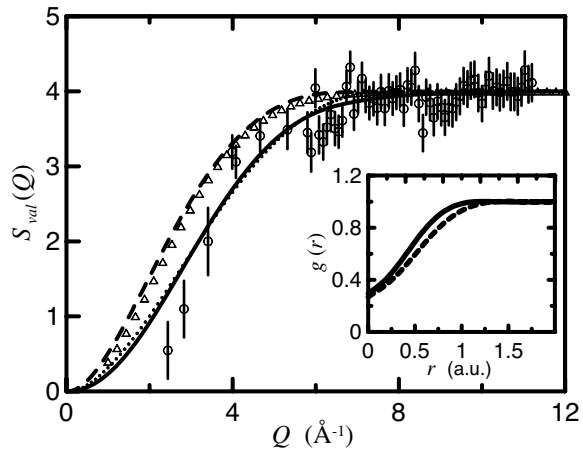

FIG. 5. Experimental static structure factor $S_{val}(Q)$ of the valence electrons in C_{60} (circles, present experiment) and diamond (empty triangles, experiment of Ref. 7). Calculated static structure factor of the valence electrons in C_{60}: dotted line, homogeneous interacting electron gas model at the best fitting value $r_s = 0.99$; dashed line, LDA for $w(Q;n(\mathbf{r}))$; continuous line, beyond-LDA for $w(Q;n(\mathbf{r}))$ (see Eq. (6)). Inset: model pair correlation function $g(r)$ in C_{60} (continuous line) and diamond[7] (dashed line).

The present experimental data of $S_{val}(Q)$ in C_{60} can be interpreted within the interacting homogeneous electron-gas model. We exploited the approach developed in Ref. 17, which is based on an accurate fit of the simulation data of Ref. 18. By varying the electron-gas parameter r_s, which is defined by $r_s=[3/(4\pi n_0 a_B^3)]^{1/3}$, n_0 being the electron density and a_B the Bohr radius, we selected the r_s value corresponding to the electron-gas static-structure factor, which provides the best agreement with the experimental $S_{val}(Q)$ in fullerene, namely, $r_s=0.99\pm0.05$. In Fig. 5 the experimental $S_{val}(Q)$ are compared with the static-structure factor of the electron gas as resulting from the best-fit choice $r_s=0.99$. We remark that $r_s=0.99$ corresponds to an average valence-electron density significantly larger than that associated to the actual average fullerene density, which is consistent with $r_s=1.47$. These values should be compared with the companion data in diamond,[7] where $r_s=1.2$ resulted from the fit based on the electron-gas model against 1.32 from the average diamond density. The results of the electron-gas model seem to indicate a higher degree of electron localization in C_{60} fullerene than in diamond, that is, the C_{60} spheres behave like rather a compact structure if compared with the relatively open structure of diamond. The rather high value of the average valence-electron density in C_{60} is consistent with an electron distribution that is peaked inside a layer around the fullerene and decreasingly low in the interstitial region.

The analysis of the static-structure factor based on the model of the homogeneous interacting electron gas[17,18] can be expanded by following a density-functional approach to the interacting electron system within either the LDA or beyond-LDA schemes. Indeed, the static-structure factor was written as

$$S_w(Q) = \int_{\Omega_0} d\mathbf{r} w[Q;n(\mathbf{r})] S_h[Q;n(\mathbf{r})], \tag{5}$$

where $S_h[Q;n(\mathbf{r})]$ is the static-structure factor of the homogeneous electron system with density $n(\mathbf{r})$ and $w[Q;n(\mathbf{r})]$ is an appropriate weight function that depends on Q and $n(\mathbf{r})$. The integral is over the atomic volume Ω_0. The usual LDA scheme for the exchange-correlation potential is recovered for the choice

$$w[Q;n(\mathbf{r})] = n(\mathbf{r}).$$

We observe that the LDA prescription provides a static-structure factor which has the correct behavior in the limit $Q\to\infty$, although it fails in satisfying the low-momentum sum rule[19]

$$\lim_{Q\to 0} S(Q) \sim \frac{Z\hbar Q^2}{2m\omega_p},$$

where $\omega_p^2=4\pi e^2 Z/(m\Omega_0)$ is the *unperturbed* plasma frequency associated to free electronlike oscillations of the valence electrons. The value used here for the reference frequency ω_p is that appropriate to the homogeneous electron gas with density equal to the *average* density Z/Ω_0 of the valence electrons in C_{60}. We observe that the plasma frequency appearing in the long-wavelength sum rule represents the $Q\to 0$ limiting value of the plasmon dispersion under a random phase approximation (RPA) treatment of the homogeneous electron gas. The validity of the sum rule on the static-structure factor $S(Q)$, which is the energy integral of the dynamic-response function $S(Q,\omega)$, stems from the assumption that in the long-wavelength limit the response function is dominated by the contribution of almost undamped plasmons over quasiparticle excitations.[19] This assumption, which applies correctly to the electron liquid, can be extended to the case of valence electrons in solids whenever the plasma frequency is higher than both the maximum frequency associated to interband transitions and the frequency related to the energy gap. In the present context, however, the frequency ω_p should not be related to the plasmon features of the excitation spectrum as measured in C_{60} fullerenes.[20] In the limit $Q\to 0$, a simple and appropriate expression for the weight function would be

$$w[Q;n(\mathbf{r})] = \sqrt{\frac{\Omega_0 n^3(\mathbf{r})}{Z}}.$$

Therefore, a sensible approximation to $w[Q;n(\mathbf{r})]$, which were valid at every Q while providing the correct low-Q and high-Q limiting behavior, would be

$$w[Q;n(\mathbf{r})] = \exp(-\alpha Q^2/k_F^2)\sqrt{\frac{\Omega_0 n^3(\mathbf{r})}{Z}} + [1-\exp(-\alpha Q^2/k_F^2)]n(\mathbf{r}), \tag{6}$$

which is correct also in the case of the homogeneous electron system. In Eq. (6), α is a constant and $k_F=k_F[n(\mathbf{r})]$ is the Fermi wave vector, which is calculated in each point by using the corresponding local-valence electron density according to the LDA prescription. We applied Eq. (5) to model the

static-structure factor of valence electrons in fullerene, under both the LDA prescription and the scheme beyond-LDA as provided by Eq. (6). In the latter case, the α constant was determined by fitting $S_w(Q)$ to the diamond data[7] and the resulting value, namely, $\alpha = 0.45$, was held fixed in the calculation of $S_w(Q)$ for fullerene. The electron density $n(\mathbf{r})$ in both fullerene and diamond was modeled by the appropriate superpositions of the free-carbon-atom electron densities, as given by the relativistic Hartree-Fock calculations of Ref. 21.

The so-calculated static-structure factors are shown in Fig. 5, where it is evident the close similarity between the electron-gas analysis[17,18] and the calculation beyond-LDA, whereas the LDA approach strikingly fails in modeling the experimental data of C_{60}. To complement the information obtained in the momentum space, in the inset of Fig. 5 we show the pair-correlation function as calculated in the homogeneous electron-gas scheme at the electron density corresponding to the best fit of the $S_{val}(Q)$ in fullerene (r_s=0.99). The same function, as obtained in diamond, is also shown for comparison purposes. We observe that the pair-correlation function in diamond has quite a similar shape to that of fullerene, although the size of the excluded volume is smaller in C_{60} than in diamond corresponding to a larger effect of the electron-electron interactions.

IV. CONCLUSION

The results here obtained in C_{60}, despite the intrinsic experimental difficulties and the limited information available from literature, enabled a meaningful and consistent determination of the exchange-correlation energy, which was found to be larger in fullerene than in diamond. This result indicates that the stability of fullerene is largely brought about by the exchange-correlation term of the electron interaction and, for a complete description of the ground-state energy of this system, the measurement of the electron-density distribution, although made complex by the presence of the orientational disorder, is mandatory. We remark that for a complete picture of the energy diagram of the carbon allotropes, that is, ground state and cohesive energy versus structure and coordination, the measurement of the static structure factor in graphite and carbon nanotubes should be carried out.

A clear indication came out from the present data about the validity extent of the LDA treatment of the electron correlations. Indeed, the LDA inadequacy in providing a reliable description of the pair-correlation function, that is a many-electron ground-state property, is apparent here. Therefore, despite the fact that LDA is widely proven to be a meaningful and properly working approximation for ground-state properties of slowly varying density systems, a scheme beyond-LDA is necessary to model the electron density in fullerene, which is notably varying from the center and along the radius of the fullerene. Moreover, the failure of the LDA in reproducing the pair-correlation function in fullerene could be linked up to the highly correlated electron nature of this system. This suggestion couples with the recognized drawback of the LDA in reproducing the one-electron band structure and the excited states in C_{60}. In literature, evidence of the LDA approach failing to properly describe the electron-energy states and excitation spectra in highly correlated systems are reported. In the specific case of fullerenes, numerous investigations on electron states and electronic structure have been carried out[22] and a recent review of the experimental results obtained by electron spectroscopy techniques is given in Ref. 23, together with a discussion on the importance of these techniques in the understanding of the electron interactions. We mention that time-dependent density-functional calculations have been used to interpret the photoexcitation spectrum in C_{60} ions.[20]

As a final remark we observe that the present results suggest that the existence of the different carbon allotropes is intimately related to the exchange-correlation energy dependence on the valence-electron density. This dependence seems to be confirmed by the results of a quantum-diffusion Monte Carlo calculation[24] on the binding energies for different isomers of carbon clusters with variable size.

[1] G. Mazzone and F. Sacchetti, Phys. Rev. B **30**, 1739 (1984).
[2] C. Petrillo, F. Sacchetti, and G. Mazzone, Acta Crystallogr., Sect. A: Found. Crystallogr. **54**, 468 (1998).
[3] P. Hohenberg and W. Kohn, Phys. Rev. **136**, B864 (1964); W. Kohn and L. J. Sham, Phys. Rev. **140**, A1133 (1965); O. Gunnarsson, M. Jonson, and B. I. Lundqvist, Phys. Rev. B **20**, 3136 (1979).
[4] G. Mazzone, F. Sacchetti, and V. Contini, Phys. Rev. B **28**, 1772 (1983).
[5] C. B. Walker, Phys. Rev. **103**, 558 (1956).
[6] T. Paakkari and P. Suortti, Phys. Rev. B **9**, 1756 (1974).
[7] C. Petrillo and F. Sacchetti, Phys. Rev. B **51**, 4755 (1995).
[8] G. Calzuola, C. Petrillo, and F. Sacchetti, Phys. Rev. B **59**, 12853 (1999).
[9] M. F. Jarrold, Nature (London) **407**, 26 (2000).
[10] A. N. Khlobystov, D. A. Britz, A. Ardavan, and G. A. Briggs, Phys. Rev. Lett. **92**, 245507 (2004).
[11] O. Blaschko, G. Krexner, Ch. Maier, and R. Karawatzki, Phys. Rev. B **56**, 2288 (1997).
[12] S. L. Chaplot, L. Pintschovius, M. Haluska, and H. Kuzmany, Phys. Rev. B **51**, 17028 (1995).
[13] F. Leclercq, P. Damay, M. Foukani, P. Chieux, M. C. Bellissent-Funel, A. Rassat, and C. Fabre, Phys. Rev. B **48**, 2748 (1993).
[14] J. Z. Liu, J. W. Dykes, M. D. Lan, P. Klavins, R. N. Shelton, and M. M. Olmstead, Appl. Phys. Lett. **62**, 531 (1993).
[15] R. T. Brown, Phys. Rev. A **5**, 2141 (1972).
[16] A. J. Thakkar and V. H. Smith, Jr, J. Phys. B **11**, 3803 (1978).
[17] P. Gori-Giorgi, F. Sacchetti, and G. B. Bachelet, Phys. Rev. B **61**, 7353 (2000).
[18] G. Ortiz, M. Harris, and P. Ballone, Phys. Rev. Lett. **82**, 5317 (1999).
[19] D. Pines and Ph. Nozieres, *The Theory of Quantum Liquids* (W.

A. Benjamin Inc., New York, 1966).
[20] S. W. J. Scully, E. D. Emmons, M. F. Gharaibeh, R. A. Phaneuf, A. L. D. Kilcoyne, A. S. Schlachter, S. Schippers, A. Muller, H. S. Chakraborty, M. E. Madjet, and J. M. Rost, Phys. Rev. Lett. **94**, 065503 (2005), and references therein.
[21] P. A. Doyle and P. S. Turner, Acta Crystallogr., Sect. A: Cryst. Phys., Diffr., Theor. Gen. Crystallogr. **24**, 390 (1968).
[22] R. W. Lof, M. A. van Veenendaal, B. Koopmans, H. T. Jonkman, and G. A. Sawatzky, Phys. Rev. Lett. **68**, 3924 (1992).
[23] P. Rudolf, M. S. Golden, and P. A. Bruhwiler, J. Electron Spectrosc. Relat. Phenom. **100**, 409 (1999). and references therein.
[24] P. R. C. Kent, M. D. Towler, R. J. Needs, and G. Rajagopal, Phys. Rev. B **62**, 15394 (2000).